JOURNAL OF SPACECRAFT AND ROCKETS
Vol. 35, No. 6, November–December 1998

Flush Air Data System Calibration Using Numerical Simulation

Ian A. Johnston* and Peter A. Jacobs†
University of Queensland, Brisbane, Queensland 4072, Australia
and
Takayuki Shimoda‡
National Space Development Agency, Tsukuba City, Ibaraki 305, Japan

The use of computational fluid dynamics simulations for calibrating a flush air data system is described. In particular, the flush air data system of the HYFLEX hypersonic vehicle is used as a case study. The HYFLEX air data system consists of nine pressure ports located flush with the vehicle nose surface, connected to onboard pressure transducers. After appropriate processing, surface pressure measurements can be converted into useful air data parameters. The processing algorithm requires an accurate pressure model, which relates air data parameters to the measured pressures. In the past, such pressure models have been calibrated using combinations of flight data, ground-based experimental results, and numerical simulation. We perform a calibration of the HYFLEX flush air data system using computational fluid dynamics simulations exclusively. The simulations are used to build an empirical pressure model that accurately describes the HYFLEX nose pressure distribution over a range of flight conditions. We believe that computational fluid dynamics provides a quick and inexpensive way to calibrate the air data system and is applicable to a broad range of flight conditions. When tested with HYFLEX flight data, the calibrated system is found to work well. It predicts vehicle angle of attack and angle of sideslip to accuracy levels that generally satisfy flight control requirements. Dynamic pressure is predicted to within the resolution of the onboard inertial measurement unit. We find that wind-tunnel experiments and flight data are not necessary to accurately calibrate the HYFLEX flush air data system for hypersonic flight.

Nomenclature

$\boldsymbol{A}$ = design matrix
$\boldsymbol{b}$ = residual vector
c = polynomial coefficient
E = residual pressure error, Pa
F = generalized surface pressure model, Pa
f = pressure correction function
g = component of f
i = pressure port label
M = Mach number
$\boldsymbol{n}$ = surface normal vector
P = surface pressure, Pa
p = component of f
q = dynamic pressure, Pa
$\boldsymbol{q}$ = air data state vector
R = pressure ratio
α = angle of attack, deg
β = angle of sideslip, deg
γ = specific heat ratio
θ = local flow incidence angle, rad
λ = scale factor
σ = pressure measurement standard deviation, Pa

Subscripts

a = amplitude
g = gauge
k = polynomial coefficient index
t = total (stagnation)
0 = standard condition
∞ = freestream

Superscripts

j = iteration number
$*$ = best estimate
$\hat{}$ = unit vector

Received Feb. 25, 1998; revision received June 29, 1998; accepted for publication July 1, 1998.

*Ph.D. Student, Department of Mechanical Engineering. Student Member AIAA.
†Senior Lecturer, Department of Mechanical Engineering.
‡Associate Senior Engineer, Office of Research and Development, Tsukuba Space Center, 2-1-1 Sengen.

Introduction

THE successful control of a hypersonic vehicle in flight requires knowledge of the vehicle state to sufficient accuracy. Particularly important are the state data that describe the ambient atmosphere and its interaction with the moving vehicle. These are often called air data and can be used to evaluate quantities such as the pressure loading and heat loading on the vehicle. Air data may also be used to determine the pressure altitude and attitude of the vehicle, assisting the control system to keep the vehicle trajectory within the desired flight envelope. Examples of air data parameters include angle of attack, angle of sideslip, freestream dynamic pressure, and freestream static pressure. For flight experiments, accurate knowledge of these kinds of air data parameters is crucial in the postflight reconciliation of flight measurements with ground-based experiments and computational fluid dynamics (CFD) predictions.[1]

There are several types of instrumentation available for measuring air data, many of them reviewed in Ref. 2. Laser velocimeter systems are reported to have good accuracy but do not work well at high altitude and are unable to produce a full set of air data information.

Alternatively, information from onboard inertial measurement units (IMU) can be used to infer air data. IMU gyroscopes and accelerometers are used to compute estimates of vehicle velocity, altitude, and attitude with respect to a fixed coordinate system. In conjunction with an aerodynamic model of the vehicle, the IMU data can also be used to estimate atmospheric conditions. The IMU computed air data are prone to a number of error sources; apart from the effects of IMU instrument drift and inaccuracies in the vehicle aerodynamic model, the computed air data do not usually account for local wind speed. Supplementing the IMU computed air data with positional and meteorological information derived from satellites can improve their accuracy.

A third method for the determination of air data is a technique based on flowfield pressure measurement. For subsonic and supersonic craft, this may be performed with a flow-intrusive boom instrumented with a pitot tube and mechanical vanes.[3] However, the

high-energy nature of hypersonic flow makes an intrusive boom impractical because it would quickly become damaged. Additionally, an intrusive boom disrupts the flow pattern around the vehicle and can lead to flight instabilities for some craft.[4] A remedy to this is the flush air data system concept (FADS), which consists of a number of pressure tappings located flush with the vehicle surface, usually near the nose. The measured distribution of the pressure field around the nose is then used to infer the air data. A minimum of four pressure ports is needed to obtain a complete set of air data parameters, although more ports will increase accuracy. Improvements in accuracy start to diminish when more than nine ports are used.[5]

For hypersonic flows, modified Newtonian theory is able to reasonably predict vehicle surface pressures as a function of air data. Thus, by solving an inverse problem, the theory can be used to determine the air data in terms of the known surface pressure measurements. The simplicity and robustness of modified Newtonian theory make it ideal for use in a hypersonic FADS. However, the accuracy of modified Newtonian theory may not be sufficient for all FADS applications.

There are two main approaches in achieving increased accuracy in air data prediction. The first is to apply correction factors to the air data parameters predicted by the FADS but retain the underlying modified Newtonian pressure model. This method has been used extensively in the past.[6] The second approach is more fundamental: A better pressure model is created by applying correction factors directly to the Newtonian theory. It is this second technique that will be used to calibrate an entry vehicle FADS in this paper. The calibration involves finding sets of correction factors applicable to different flight conditions experienced by the vehicle. The correction factors compensate for high-temperature gas effects, boundary-layer growth, the bow shock wave, and other real flow phenomena not modeled by modified Newtonian theory.

For both approaches, the correction factors can be determined from flight experiments, ground-based experiments, CFD, or analytical flow theory. Undoubtedly, flight-generated correction factors are the most desirable, but they are unavailable for maiden flights and single-use vehicles. Correction factors may be obtained from ground-based experiments, such as wind-tunnel tests,[7] but these may not cover the entire flight envelope or provide sufficient accuracy and are subject to the effects of scale.[8] Additionally, a large number of ground-based experiments are needed, and performing them can be time consuming and costly. Using a validated CFD solver to generate a suite of correction factors is an attractive option due to its wide range of applicability, low cost, and very high precision. The accuracy of a CFD solver, though, must be ascertained before it is relied on.

We will examine a FADS calibration technique that involves the determination of correction factors using only CFD. The proposed method involves correcting the underlying pressure model exclusively, rather than correcting the predicted air data. This procedure will subsequently be applied to generate air data parameters from FADS pressure data collected by the hypersonic flight experiment (HYFLEX) entry vehicle. The air data parameters predicted by the CFD-calibrated FADS will be compared to IMU results. It will be shown that this solely numerical calibration procedure provides air data that are generally accurate enough for hypersonic vehicle control requirements. Comparison will also be made against air data parameters predicted by an uncalibrated FADS based on modified Newtonian theory.

HYFLEX Project

The Japanese National Aerospace Laboratory and National Space Development Agency undertook the HYFLEX project to gather data on entry vehicle aerodynamics and aerothermodynamics.[9] In February 1996, the HYFLEX vehicle successfully performed an aerobraking maneuver to decelerate and descend to sea level from an initial height of 110 km and Mach number of 13. A diagram of the HYFLEX is shown in Fig. 1. The vehicle was approximately 4 m long, with a nose radius of 0.4 m. Also visible in Fig. 1 are the nine FADS pressure ports located in a cruciform array on the nosecap, together with their corresponding labels.

Although the HYFLEX was instrumented with FADS pressure sensors, they were not employed during the flight to determine air data parameters. Instead, the FADS pressure measurements were transmitted to surface receivers to be used for postflight analysis. During flight, an IMU was used to compute air data parameters for control purposes.[10]

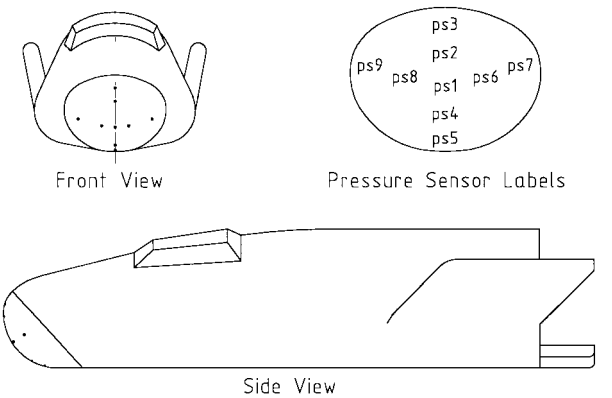

Fig. 1 HYFLEX vehicle and nose pressure port layout.

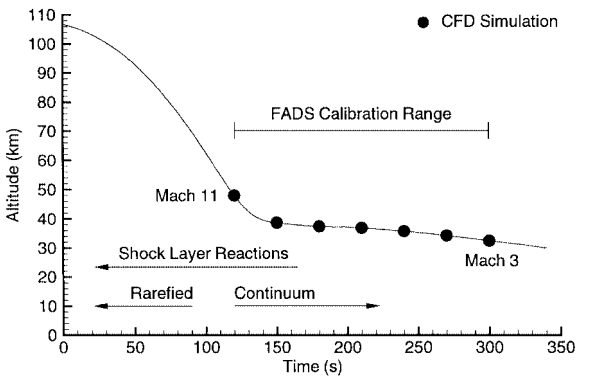

Fig. 2 HYFLEX time–altitude map.

The HYFLEX descent time–altitude map is shown in Fig. 2. At approximately 120 s after separation, the vehicle enters the continuum flow flight regime and is traveling at 3.74 km/s (Mach 11.4). High-temperature gas effects in the shock layer, including chemical nonequilibrium, are strong at this time. By about 170 s after separation, the high-temperature effects are weak, and the vehicle has decelerated to 2.28 km/s (Mach 7.1). At 300 s, the vehicle speed is 0.90 km/s (Mach 2.9). For the scope of this work, the HYFLEX FADS will be calibrated for operation over the range of flight conditions encountered during the period 120–300 s after separation. In the rarefied and transitional flow experienced before 120 s, pressure sensor error constitutes a significant proportion of the measured pressures. Pressure measurements made during this time are, thus, less useful as test data for the comparison of FADS calibration techniques.

Air Data Inverse Problem

The surface pressure distribution over the HYFLEX is a function of a large set of variables, including the entire vehicle geometry. However, we may approximate the surface pressures at the nose pressure ports by the following functional relationship:

$$P_i \cong F_i(P_{gt}, P_\infty, \alpha, \beta; \hat{\boldsymbol{n}}_i) \tag{1}$$

where i represents the pressure port and F_i is a function estimating the surface pressure P_i at this pressure port location. The vector $\hat{\boldsymbol{n}}_i$ is the unit normal to the surface at location i, measured in a vehicle frame of reference. This vector is easily measured before flight and can be considered a known quantity. P_{gt} is the gauge pressure at the stagnation point on the vehicle surface, equal to the stagnation pressure P_t minus the freestream static pressure P_∞. The vehicle angle of attack is α, and the sideslip angle is β. Most other air data of interest, including freestream dynamic pressure and Mach number, can be calculated from these four parameters.

A procedure for solving for the four unknown air data parameters (P_{gt}, P_∞, α, and β) is now presented. Given that nine pressure observations are available on the HYFLEX, we may construct the following system of nine equations:

$$P_i = F_i\left(P^*_{gt},\, P^*_\infty,\, \alpha^*,\, \beta^*;\, \hat{\boldsymbol{n}}_i\right) + E^*_i, \qquad i = 1, 2, \ldots, 9 \quad (2)$$

The quantity P_i is the surface pressure measured by sensor i, and P^*_{gt}, P^*_∞, α^*, and β^* are the unknown air data parameters that best fit the available set of pressure observations. For nine pressure sensors, there are more equations than unknowns, and solution requires the inversion of an overconstrained system. In general, it is not possible to solve the system exactly, and residual errors E^*_i will remain. Thus, some kind of error minimization technique must be employed to invert the system. The method of least squares is commonly used for minimizing error in overdetermined systems,[11] and this technique has also been used before in FADS applications.[5]

Least squares can be performed quickly and easily on linear systems. However, for the nonlinear equation set (2), the equations must first be linearized and an iterative technique applied. Let the jth guess for the best state vector of air data parameters be $\boldsymbol{q}^j = [P^j_{gt}\ \ P^j_\infty\ \ \alpha^j\ \ \beta^j]^T$. The guess is then improved iteratively by applying

$$\boldsymbol{q}^{j+1} = \boldsymbol{q}^j + \delta\boldsymbol{q} \quad (3)$$

until $\boldsymbol{q}^j = \boldsymbol{q}^*$. In practice this is attained when estimate j is close to estimate $j+1$.

At each iteration step, the incremental term $\delta\boldsymbol{q}$ in Eq. (3) must be evaluated. Consider a Taylor series expansion of the F_i about state j and neglect terms higher than first order. We may then write

$$\boldsymbol{b} = \boldsymbol{A}\delta\boldsymbol{q} \quad (4)$$

where

$$\boldsymbol{A} = \begin{bmatrix} \frac{1}{\sigma_1}\frac{\partial F_1}{\partial P_{gt}} & \frac{1}{\sigma_1}\frac{\partial F_1}{\partial P_\infty} & \frac{1}{\sigma_1}\frac{\partial F_1}{\partial \alpha} & \frac{1}{\sigma_1}\frac{\partial F_1}{\partial \beta} \\ \vdots & \vdots & \vdots & \vdots \\ \frac{1}{\sigma_i}\frac{\partial F_i}{\partial P_{gt}} & \frac{1}{\sigma_i}\frac{\partial F_i}{\partial P_\infty} & \frac{1}{\sigma_i}\frac{\partial F_i}{\partial \alpha} & \frac{1}{\sigma_i}\frac{\partial F_i}{\partial \beta} \\ \vdots & \vdots & \vdots & \vdots \\ \frac{1}{\sigma_9}\frac{\partial F_9}{\partial P_{gt}} & \frac{1}{\sigma_9}\frac{\partial F_9}{\partial P_\infty} & \frac{1}{\sigma_9}\frac{\partial F_9}{\partial \alpha} & \frac{1}{\sigma_9}\frac{\partial F_9}{\partial \beta} \end{bmatrix}_{\boldsymbol{q}^j} \quad (5)$$

and

$$\boldsymbol{b} = \begin{bmatrix} \frac{E^j_1}{\sigma_1} & \cdots & \frac{E^j_i}{\sigma_i} & \cdots & \frac{E^j_9}{\sigma_9} \end{bmatrix}^T \quad (6)$$

In Eqs. (5) and (6), $\boldsymbol{A}$ and $\boldsymbol{b}$ are referred to as the design matrix and residual vector, respectively. The weighting terms σ_i represent the standard deviation in pressure measurement uncertainty for sensor i. It is assumed here that all pressure sensors have equal uncertainty. To find $\delta\boldsymbol{q}$, we multiply both sides of Eq. (4) by $\boldsymbol{A}^{-1}$:

$$\delta\boldsymbol{q} = \boldsymbol{A}^{-1}\boldsymbol{b} \quad (7)$$

Because $\boldsymbol{A}$ is a nonsquare matrix, its inverse is undefined. The matrix $\boldsymbol{A}^{-1}$ is, thus, referred to as the pseudoinverse of $\boldsymbol{A}$. To solve the least-squares problem for $\delta\boldsymbol{q}$, we now need the pseudoinverse of the design matrix that minimizes the 2-norm of the residual vector.

There are several techniques available to accomplish this task. Singular value decomposition (SVD) is one of the most robust and can be applied to decompose $\boldsymbol{A}$ into the product of a series of component matrices that are easily inverted. The technique is described in many numerical analysis texts[11] and will not be repeated here. Although SVD is not the fastest way to solve the least-squares problem, it provides useful information about the conditioning of the design matrix and the relative importance of solution components.

The partial derivatives in Eq. (5) are easily found if F_i is a simple analytical function. For more complex functions, the derivatives are evaluated numerically. The numerical approximation to the partial derivative of F_i with respect to any air data parameter x is

$$\left.\frac{\partial F_i}{\partial x}\right|_j \approxeq \frac{F_i(x^j + \Delta) - F_i(x^j)}{\Delta} \quad (8)$$

where Δ is a small number, such that Δ/x^j is a few orders of magnitude greater than machine precision (for $x^j \neq 0$).

If the measured pressure data contain spikes or irregularities or a very poor initial guess $\boldsymbol{q}^1$ is made, then the iterations may not converge. Nonconvergence is usually manifested in the guesses for $\boldsymbol{q}$ oscillating about (but not approaching) $\boldsymbol{q}^*$. If convergence is not reached within a reasonable number of iterations, a semi-implicit technique is employed to attempt to regain stability. This technique involves calculating all of the partial derivatives in $\boldsymbol{A}$ with Eq. (8) while setting Δ to the corresponding value of the air data parameter in the most recently computed $\delta\boldsymbol{q}$. Equation (7) is then used to find a better $\delta\boldsymbol{q}$. New derivatives for $\boldsymbol{A}$ are recalculated using the new $\delta\boldsymbol{q}$ as values of Δ in Eq. (8), and the procedure is repeated several times. Once the optimum value of $\delta\boldsymbol{q}$ is finally found, it is substituted into Eq. (3) to update the state vector estimate. The semi-implicit technique then remains in use until convergence is obtained.

Once the best air data state vector $\boldsymbol{q}^*$ is determined, the known air data parameters are used to compute other air data of interest. The freestream dynamic pressure q_∞ is determined by solving the Rayleigh–Pitot equation. This equation describes the process of a thermally perfect gas passing through a normal shock and then isentropically slowing until stationary. It relates the freestream dynamic and static pressures to the postshock gauge stagnation pressure by

$$1 + \frac{P_{gt}}{P_\infty} = \left[\frac{(\gamma+1)(q_\infty/P_\infty)}{\gamma}\right]^{\gamma/(\gamma-1)} \times \left[\frac{\gamma+1}{4(q_\infty/P_\infty) - (\gamma-1)}\right]^{1/(\gamma-1)} \quad (9)$$

Real air, when processed through a strong shock and stagnated, does not keep constant γ and is not accurately described by the Rayleigh–Pitot equation. Allowances for this are described in a later section, when CFD-determined correction factors are used to remove this error source.

Mach number, if required, is easily calculated from the estimates of freestream static and dynamic pressure:

$$M_\infty = \sqrt{2q_\infty/\gamma P_\infty} \quad (10)$$

Surface Pressure Models

In the described air data system algorithm, the most critical factor affecting accuracy is the surface pressure model. If the assumed relationship between air data parameters and surface pressure is not correct, then the air data estimates will be poor.

Newtonian theory is a simple and reasonably accurate surface pressure model. The theory assumes that the freestream flow directly impacts onto the vehicle surface, transfers all momentum in the surface-normal direction to the body, and retains tangential momentum. The normal momentum flux is, thus, representative of the surface pressure, according to the theory. Most of the error in Newtonian theory arises because it is a panel method: It does not model interactions within the flow. Also, the theory does not account for boundary-layer development, shock waves, or high-temperature gas effects. Best results are obtained for hypervelocity flows, when the shock shape closely follows the body shape and the standoff distance is small; otherwise, flow interactions within the shock layer may invalidate the Newtonian assumptions. Newtonian theory does not usually predict the correct stagnation pressure and can be improved by introducing a scaling term to rectify the problem. This is called modified Newtonian theory and is written as

$$F_i = P_{gt}\cos^2\theta + P_\infty \quad (11)$$

where

$$\cos\theta = \begin{bmatrix} -\cos\alpha\cos\beta \\ \sin\beta \\ -\sin\alpha\cos\beta \end{bmatrix} \cdot \hat{\boldsymbol{n}}_i \tag{12}$$

The intermediate variable θ denotes the angle between the local (outward-facing) surface normal and the freestream flow.

The actual pressure distribution around the HYFLEX nose does not follow the Newtonian cosine-squared law. We introduce a correction factor function f into Eq. (11) to further improve its accuracy:

$$F_i = P_{gt}[\cos^2\theta + f(\theta, R, \alpha, i)] + P_\infty \tag{13}$$

where

$$R = \frac{P_\infty}{P_{gt} + P_\infty} \tag{14}$$

The correction function is introduced as an additive (rather than multiplicative) term, so that the accuracy of the formulation is not degraded when $\cos\theta$ approaches zero. The functional dependence of f on θ reflects that the correction factor varies with flow incidence angle. Likewise, nonuniformity in some of the HYFLEX nose geometry necessitates the dependence of f on the pressure port identification number i and angle of attack α. The variable R is used to give the correction function an indication of the severity of high-temperature gas effects and the nature of the flowfield. The variable is conveniently expressed in terms of already available air data parameters through Eq. (14). In the hypersonic limit, it can be deduced that R roughly scales with M_∞^{-2}. Because stagnation enthalpy is approximately proportional to M_∞^2, it can be concluded that R is roughly inversely proportional to the total temperature in the shock layer.

The value of the pressure correction function f for a particular set of arguments (θ, R, α, i), can be found by evaluating the difference between the modified Newtonian pressure prediction and the pressure determined from another, more accurate, source. By repeating this procedure over a large argument domain, the complete correction function will eventually be described. Here, the correction function will be developed by comparing the modified Newtonian theory with a number of CFD simulations. It is emphasized that no ground-based experiment data or flight pressure data are used to augment the pressure correction model. Accordingly, hereinafter Eq. (13) will be referred to as a CFD pressure model.

To determine the form of f over a large enough domain, a CFD code was used to compute the HYFLEX nose pressures for a range of different flight conditions that occurred on the actual trajectory. Figure 2 shows the seven points on the flight trajectory that were simulated. Thus, we know that seven flight conditions are guaranteed to be in the domain of f. The question then arises: Is it valid for pressure data, recorded during the flight, to be used as input to test a FADS algorithm that is based on a CFD pressure model that was calibrated for that same flight's trajectory? It is an important question, inasmuch as fair evaluation of the CFD pressure model in the results section depends on it. The validity of the on-trajectory calibration can be justified with two arguments. First, the actual flight trajectory was so close to the planned trajectory[9] that no real a posteriori accuracy advantage is gained by calibrating on flight trajectory conditions. Second, it will later be demonstrated that the CFD pressure correction function produces accurate results for sample flight conditions that are significantly off trajectory. The calibration was performed on the flight trajectory simply to allow convenient comparison of CFD and flight measured pressure results without the need for further simulations.

CFD Simulations

The SF3D CFD code was used to numerically simulate flow over the HYFLEX vehicle forebody. SF3D is a three-dimensional extension of SF2D, a hybrid shock fitting and capturing code developed by Johnston and Jacobs.[12] The code employs a three-dimensional finite volume space discretization to solve the integral form of the Navier–Stokes equations over the flow domain. Although SF3D is time accurate, it is assumed (for simplicity) that the flow around the HYFLEX is instantaneously steady at all points in flight. The assumption is reasonable because only small changes in flow conditions occur over the time required for full development of the flowfield. For example, at 120 s after flight commencement, the freestream velocity changes by only 0.1 m/s (0.003%) in the equivalent of four body lengths of flow time. Importantly, the assumption allows the generation of CFD flow solutions at any point on the trajectory, independent of previous flight conditions. Simulations of steady-state flow are obtained by marching solutions through time, from an initial condition, until the solution converges. Nominally second-order time accuracy is achieved with Runge–Kutta integration.

A modified van Albada limiter is combined with MUSCL reconstruction to obtain nominally second-order spatial accuracy.[13] For the HYFLEX simulations, some finite volume cells are quite abruptly clustered close to the vehicle surface to allow the boundary layer to be adequately captured. Both the reconstruction scheme and limiter are able to account for this nonuniform cell spacing, thus reducing the detrimental impact of cell clustering on solution quality. A shock fitting technique is used to accurately resolve the bow shock shape and location. Shock fitting also ensures that the computational grid is fully utilized, by keeping all cells within the shock layer and avoiding shock smearing. The hybrid advection upwind splitting method[14] (AUSMDV), combining flux differencing and vector splitting, is used to calculate the fluxes of conserved quantities between the finite volume cells at each time step. The AUSMDV is fairly robust and accurate and at the same time computationally cheap in comparison with other flux calculators (such as Riemann solvers).

The simulated airflow is assumed to be composed of five constituent species: N, N_2, O, O_2, and NO. Nonequilibrium effects within the system are modeled with 17 finite-rate chemical reactions.[8] For the HYFLEX trajectory, the computed air temperature in the shock layer rarely exceeds 5500 K, and so the effects of ionization are ignored. The vehicle surface is assumed to be noncatalytic, nonslip, and isothermal. The surface temperature is set to 1200 K, which is a typical value for entry vehicles. Test simulations showed, however, that the surface temperature has a negligible effect on computed surface pressures. The air viscosity is calculated using Wilke's law and the Herning–Zipperer approximation for gas mixtures, with the individual species viscosities obtained from curve fits.[15] No turbulence model is used because boundary-layer transition is expected to occur well aft of the pressure port locations. The maximum Reynolds number encountered in the HYFLEX computational domain corresponds to one-quarter of the smallest Reynolds number at which transition is observed on the Space Shuttle Orbiter.[16]

Because the aim of the CFD simulations is air data system calibration, only the parts of the flow that affect the nose pressure ports need be modeled; unnecessarily simulating the entire vehicle wastes computer resources and slows computation. Figure 3 shows an example gridded flow domain used for a HYFLEX simulation. Grids typically contained 46 cells in the longitudinal direction, 45 cells in the transverse direction, and 15–25 cells in the body-normal direction. At hypersonic flight conditions, the grid covers all of the areas of subsonic flow around the nose and undersurface of the vehicle. Also, the advection Mach number on all of the grid outflow planes were large enough to prevent the outflow boundary characteristics affecting the flow around the pressure ports. The internal grid cells were constructed so that all of the nose pressure ports coincide with the center of a finite volume cell face. For low-supersonic and transonic flight regimes, the subsonic zone expands to encompass much of the vehicle, and the grid in Fig. 3 is no longer useful. However, we are concerned only with flows faster than about Mach 2.9, where the subsonic zone remains relatively small.

An example CFD result is presented in Fig. 4. Contours of pressure and pressure correction factor f are drawn on the vehicle surface. Pressure port locations are indicated by dots. For these results, the vehicle was simulated as traveling at 3.7 km/s at an altitude of 48 km, with a 32-deg angle of attack and no sideslip. Examination of Fig. 4 reveals that the correction factor contours are axisymmetric

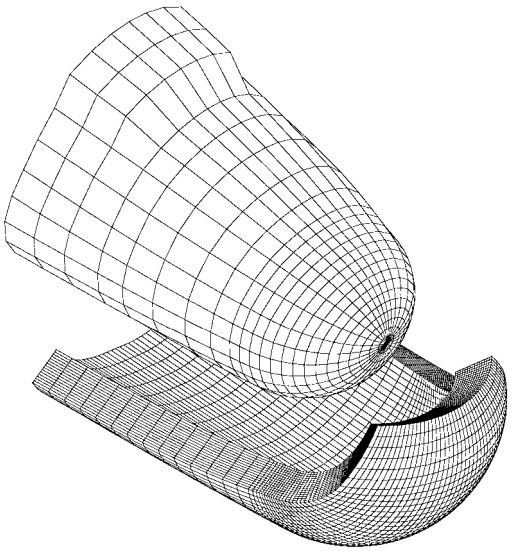

Fig. 3 Exploded view of the surface of the HYFLEX forebody and the gridded flow domain (shown without cell clustering, for clarity).

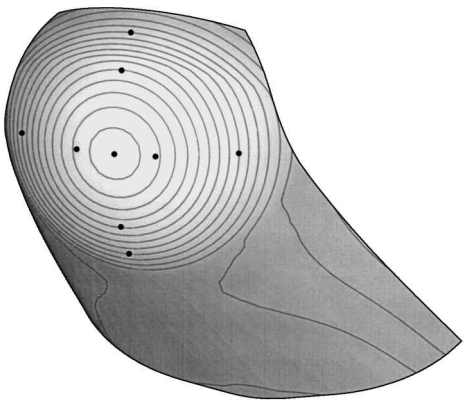

a) Pressure

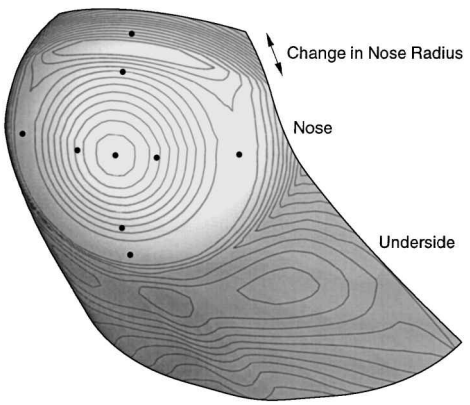

b) Pressure correction factor

Fig. 4 Contour plots of CFD results over the HYFLEX nose and underside. (Filled circles mark the locations of pressure ports.)

(about the stagnation point) over much of the nose. The axisymmetry is to be expected because the nose cap is mostly spherical. The upper pressure port (ps3), though, is located on a region of the nose where the radius of curvature decreases. This decrease in nose radius causes an increased rate of flow expansion, and the CFD result is observed to quickly depart from the modified Newtonian approximation. Pressure port ps2 is also affected by the change in nose radius, but to a lesser extent.

The axisymmetry of the correction factor contours about the stagnation point may be exploited in several ways. First, the axisymmetry indicates that f should be dependent on only one spatial variable, describing position on the nose relative to the center of symmetry. On the spherical parts of the nose, the flow incidence angle is also a measure of angular separation from the stagnation point and is an ideal choice for this variable. Second, the axisymmetry allows f to be built using fewer and simpler simulations than would be required for an asymmetric body. This is because the flow around a sphere (of radius equal to that of the HYFLEX nose) is analogous to the flow around the HYFLEX nose itself. In terms of computational requirements, the simulation of a sphere is considerably faster and easier than the simulation of the HYFLEX forebody. Results from CFD tests showed that the correction factor distribution on the sphere matched the distribution on the spherical parts of the HYFLEX nosecap. Thus, with the exception of ps2 and ps3, just one sphere flowfield is required to determine the complete form of f for a given flight condition. In total, the flow over a sphere was simulated at seven different R values, corresponding to the seven flight conditions shown in Fig. 2. These simulations were used to define the core of function f.

A different strategy was used to modify f to make allowance for the two pressure ports affected by the nonuniformity in nose cap curvature. Simulations of the HYFLEX were performed at various angles of attack and flight conditions, and the correction factors at pressure port locations ps2 and ps3 were recorded. The correction function was then amended by evaluating the difference between these values and the correction factors at equivalent incidence angles on a sphere. Overall, only about 20 simulations were used to construct f. By comparison, recent calibrations of neural-network air data systems[17] with ground-based experimental results have required well over an order of magnitude more data. The 20 CFD simulations took the equivalent of 60 days of computation on a single MIPS R10000 processor running at 195 MHz. In practice, multiple processors were used to reduce the actual time required to perform all of the simulations.

The SF3D computed correction factors are fairly small, with magnitudes typically not exceeding 0.04. As a consequence, the correction factors are especially prone to error introduced by the discretization of the flow domain. Thus, for the correction factors to be reliable, the CFD solver must be significantly more accurate than 4%. A grid convergence analysis was performed to test for numerical accuracy and is described in Ref. 8. Results showed that the average error in computed pressure (over the parts of the flow domain containing the pressure ports) was equal to 0.08% of the postshock stagnation pressure. This accuracy is good enough to render the correction factors valid.

CFD-Calibrated Surface Pressure Model

It is convenient to express the pressure correction function in terms of several component functions:

$$f = f_a(R)\,p(\lambda(R), \theta) + f_t(R) - g(R, \alpha, i) \tag{15}$$

The core of Eq. (15) is the polynomial p. It is given by

$$p = \sum_{k=1}^{4} c_k[\lambda(R)\theta]^{2k}, \qquad |\theta| \leq 1.2\,\text{rad} \tag{16}$$

with the constants $c_1 = -4.7$, $c_2 = 6.82$, $c_3 = -3.02$, and $c_4 = 0.45$ derived from CFD results. The polynomial describes the variation of the correction factor with flow incidence angle. Because the flow around the spherical part of the HYFLEX nose is axisymmetric, p is thus necessarily symmetric about the stagnation point ($\theta = 0$). Hence, p contains only even powers of θ.

A striking feature of Eq. (16) is that the curve fit coefficients c_k are constants. That is, the underlying shape of the correction function does not depend on flight conditions. Flight conditions are only needed to dictate the scaling and ordinate position of the basic polynomial p. The sensitivity to flight conditions is introduced with a single variable R [defined in Eq. (14)], which is a measure of proximity to the hypersonic limit and the strength of high-temperature effects. This variable is used as an argument to the function $\lambda(R)$, which is used to scale p with respect to θ. In a similar manner, $f_a(R)$ is used to set the amplitude of the polynomial p, according to the

Table 1 Values of various functions with respect to R

R	f_t	f_a	λ	$\frac{g(R,\alpha_0,2)}{g(R_0,\alpha_0,2)}$	$\frac{g(R,\alpha_0,3)}{g(R_0,\alpha_0,3)}$
0.0059	0.0270	0.0578	0.9278	0.7993	0.8295
0.0108	0.0157	0.0495	0.9815	1.0000	1.0000
0.0172	0.0123	0.0450	1.0010	1.2172	1.4454
0.0262	0.0094	0.0407	1.0205	1.4695	2.0202
0.0386	0.0067	0.0366	1.0337	1.7992	2.5477
0.0570	0.0038	0.0324	1.0415	2.3999	3.2533
0.0857	0.0018	0.0282	1.0292	3.2730	4.0409

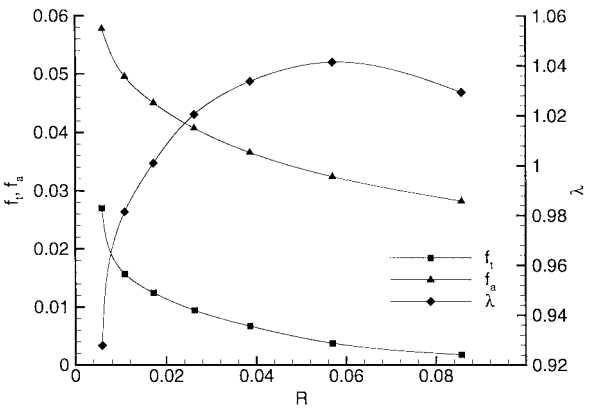

Fig. 5 Various functions against R.

flight conditions. Thus, $f_a(R)$ can be thought of as a measure of the variation in f over the body. Table 1 and Fig. 5 show the values of these functions at various R, as derived from CFD simulations.

The function $f_t(R)$ is used provide an ordinate offset, so that the correct value of f is obtained at the stagnation point ($\theta = 0$). A first examination of the CFD pressure model [Eq. (13)] indicates that f_t should be set to zero for all values of R. However, due to the inaccuracy of the Rayleigh–Pitot equation [Eq. (9)], this is not the case. The function $f_t(R)$ is used to cause the air data inversion algorithm to compute an adjusted value of P_{gt}, which, when substituted into the Rayleigh–Pitot equation, will produce the correct value of the air data parameter q_∞. In a physical sense, $f_t(R)$ may be thought of as the relative error in calculating gauge stagnation pressure with the Rayleigh–Pitot equation, as compared with a CFD calculation. Table 1 and Fig. 5 show the computed values of $f_t(R)$ for various R.

The last term in Eq. (15) is used to account for the nonuniformity in the HYFLEX nose radius. It takes the form

$$g = \begin{cases} \dfrac{g(R,\alpha_0,i)}{g(R_0,\alpha_0,i)} g(R_0,\alpha,i) & \text{for} \quad i = 2,3, \quad \beta \approx 0 \\ 0 & \text{otherwise} \end{cases} \tag{17}$$

For the pressure ports unaffected by the change in nose radius, the term vanishes. For pressure ports 2 and 3 though, the value of $g(R,\alpha,i)$ is determined using a system of two lookup tables. Table 1 shows how g varies with R at a constant value of α ($\alpha_0 = 32.7$ deg). In a like manner, Table 2 shows how g varies with angle of attack α at a constant value of R ($R_0 = 0.0108$). Using spline fits, Tables 1 and 2 are interpolated and the results combined according to Eq. (17) to find $g(R,\alpha,i)$. This procedure relies on the assumption that the behavior of g, with respect to α, scales with R. By making the assumption, it is possible to calibrate g without needing CFD results at all angles of attack at all values of R. Thus, computational effort is significantly reduced. Equation (17) also requires that the vehicle angle of sideslip is small because Table 2 was calculated with $\beta = 0$. This requirement is satisfied for the hypersonic part of the HYFLEX trajectory because β never exceeds 1 deg.

Examples of the pressure correction function at two different flight conditions are now presented. In both examples, g is ignored. The first set of conditions corresponds to 120 s after flight commencement, where the vehicle velocity is 3.7 km/s and the freestream static pressure is 97.7 Pa. For these conditions, Fig. 6

Table 2 Values of g with respect to angle of attack

α, deg:	20	30	32.7	40	50
$g(R_0,\alpha,2) \times 10^3$	11.95	6.82	4.73	1.33	1.06
$g(R_0,\alpha,3) \times 10^3$	16.21	8.75	4.17	−2.70	−5.04

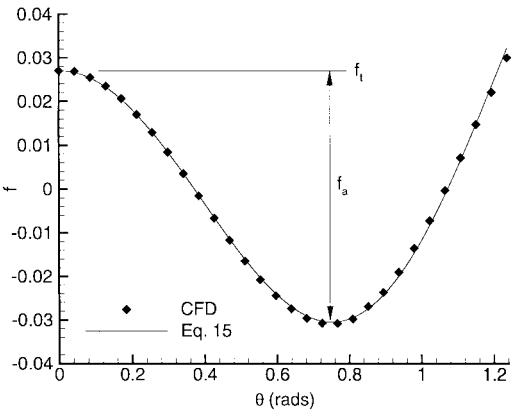

Fig. 6 Pressure correction factors for $R = 0.0059$.

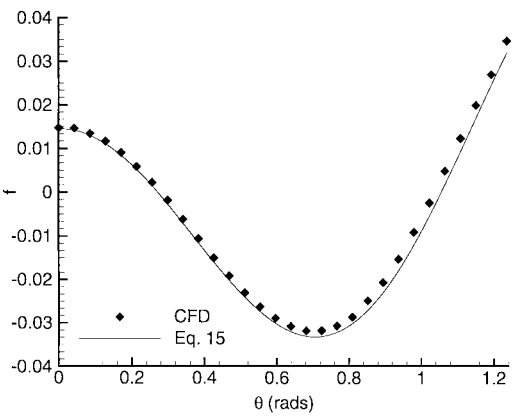

Fig. 7 Pressure correction factors for $R = 0.0130$.

shows the pressure correction factors calculated by CFD at discrete values of θ. Because these CFD results were already used in the calibration of f, we consequently see very good agreement with Eq. (15). A second set of conditions is now chosen, with a vehicle velocity of 2.5 km/s and freestream static pressure of 97.7 Pa. These conditions are significantly off the HYFLEX flight trajectory, and the pressure correction function has not been calibrated at this condition. Figure 7 shows that very good agreement between CFD results and the pressure correction function is still achieved at off-trajectory conditions.

Results and Discussion

We now test and compare the performance of the CFD-calibrated FADS algorithm with that of a FADS algorithm based on the modified Newtonian theory pressure model. The comparison is conducted over the hypersonic part of the HYFLEX trajectory, using the HYFLEX pressure measurements recorded in flight as input.

Figure 8 shows the FADS predictions and IMU measurement of vehicle angle of attack. The CFD–FADS prediction is observed to agree closely with the IMU result, whereas the Newtonian–FADS result deviates considerably from the IMU signal. A plot showing the difference between the FADS predictions and IMU result is presented in Fig. 9. The HYFLEX handbook[18] reports that the accuracy of the IMU measurement is ±0.65 deg at the point of maximum dynamic pressure (140 s after flight commencement), decreasing to ±0.45 deg at Mach 3 (about 300 s after flight commencement). These quoted accuracies represent a variation of ±3 standard deviations. Thus, with the exception of a single data spike, the CFD–FADS result is completely contained within the quoted error band, whereas the Newtonian–FADS result lies mostly outside the band.

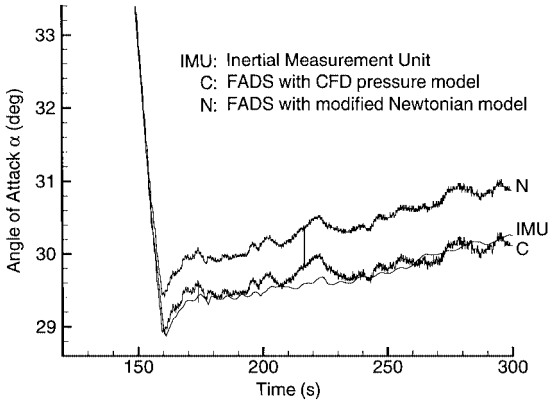

Fig. 8 Comparison of angle-of-attack predictions made by the IMU and the FADS using the CFD pressure model (C), and the modified Newtonian pressure model (N); results are shown at a 10-Hz frequency.

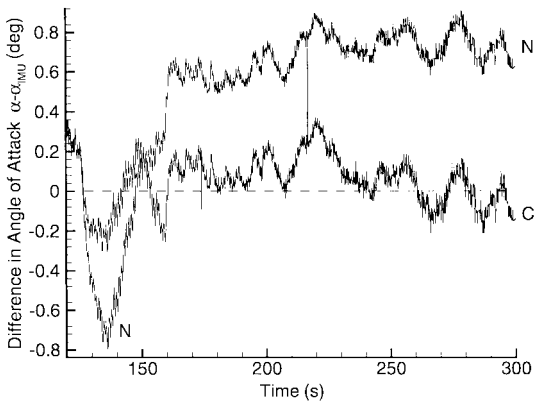

Fig. 9 Difference between the angle of attack predicted by the FADS and the IMU.

The CFD–FADS estimates of α vary from the IMU with an average bias of +0.05 deg and standard deviation of 0.13 deg. The Newtonian–FADS shows an average bias of +0.51 deg and standard deviation of 0.39 deg. For a generic, broad-envelope, hypersonic vehicle, accuracies of 0.5 deg in angle of attack are typically required.[2] The results show that this kind of accuracy can be achieved with a CFD-calibrated FADS.

The accurate CFD–FADS prediction of α is strongly dependent on the $g(R, \alpha, i)$ term in the pressure correction function [Eq. (15)]. As already described, g is used to account for the nonuniformity in nose radius near pressure ports 2 and 3. Without the inclusion of this term, it was found that the CFD–FADS estimates of α were of an accuracy similar to the Newtonian–FADS results. Thus, it appears that the inability of modified Newtonian theory to properly model ps2 and ps3 is responsible for its degraded performance in the prediction of α.

Figure 10 compares the angle of sideslip estimates made by the FADS and the IMU. The estimates made by the CFD–FADS and Newtonian–FADS algorithms are close to identical. Relative to the IMU results, the CFD–FADS has an average bias in β of −0.34 deg and a 0.17-deg standard deviation. The Newtonian–FADS has an average bias of −0.3 deg and a standard deviation of 0.16 deg. The IMU has a $\pm 3\sigma$ uncertainty in β of ±0.41 deg at 140 s and ±0.6 deg at 300 s (Ref. 18). For the control of a hypersonic vehicle, β is typically required to an accuracy of 0.5 deg (Ref. 2). For both of the FADS results, accuracy is better than 0.5 deg for the most part.

Figure 11 shows the FADS and IMU predictions of freestream dynamic pressure. Differences between the sets of data are more clearly seen in Fig. 12, which shows the FADS predictions relative to the IMU. The $\pm 3\sigma$ uncertainty in the IMU estimated q_∞ is at least ±360 Pa at 140 s and ±120 Pa at 300 s (Ref. 18). The CFD–FADS q_∞ estimates straddle the edge of the IMU error band and have an average bias of +130 Pa with a 200-Pa standard deviation. The Newtonian–FADS estimates are well outside the quoted

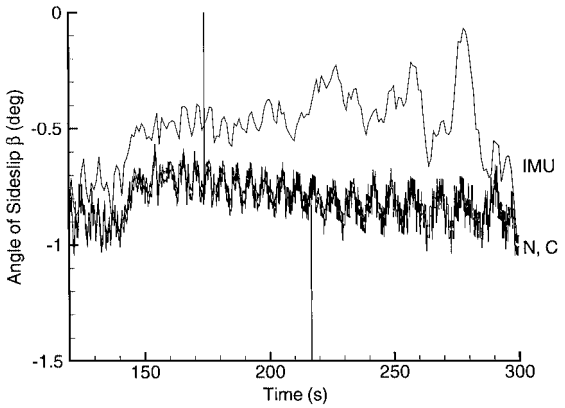

Fig. 10 Comparison of angle-of-sideslip predictions made by the IMU and the FADS.

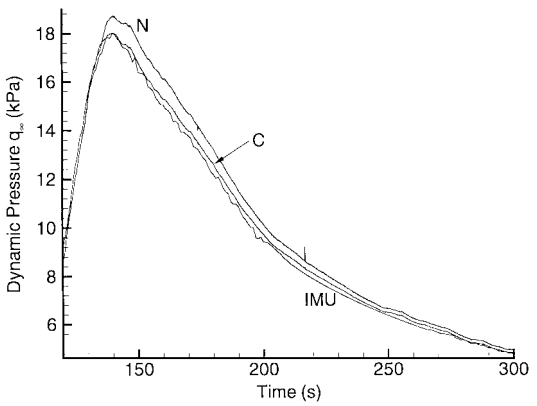

Fig. 11 Dynamic pressure predicted by the IMU compared with the predictions made by the FADS.

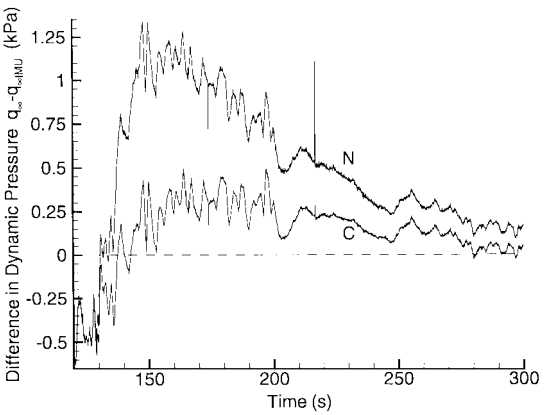

Fig. 12 Difference between the dynamic pressure predictions made by the FADS and the IMU.

band and have an average bias of +500 Pa and standard deviation of 410 Pa with respect to the IMU data. Typically, a hypersonic vehicle requires dynamic pressure to within ±1% accuracy.[2] This requirement is not met by the Newtonian–FADS. Because the resolution of the IMU roughly corresponds to ±2.5% of q_∞, it is not possible to say whether this goal was reached by the CFD–FADS.

The wind-tunnel calibration of the Shuttle entry air data system (SEADS) is described in Ref. 7. The paper includes an accuracy analysis of the SEADS for a Shuttle entry over the range from Mach 0.5 to Mach 26. The air data accuracies are presented as average values over 100-s time intervals. Over the range from Mach 2.8 to Mach 11.9, which corresponds to the HYFLEX flight speeds considered in this paper, the maximum averaged error in SEADS α and β estimates are reported to be 0.69 and 0.33 deg, respectively. The maximum averaged error in SEADS stagnation pressure is 540 Pa. (The absolute stagnation pressure corresponding to this

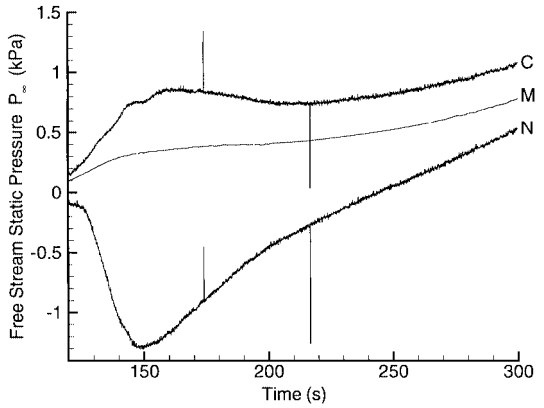

Fig. 13 Freestream static pressure estimated by the FADS compared with the atmospheric pressure determined from meteorological data (M).

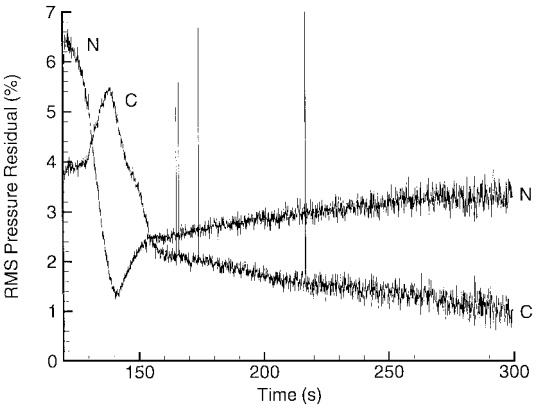

Fig. 14 RMS pressure residual for the FADS algorithm, expressed as a percentage of freestream dynamic pressure.

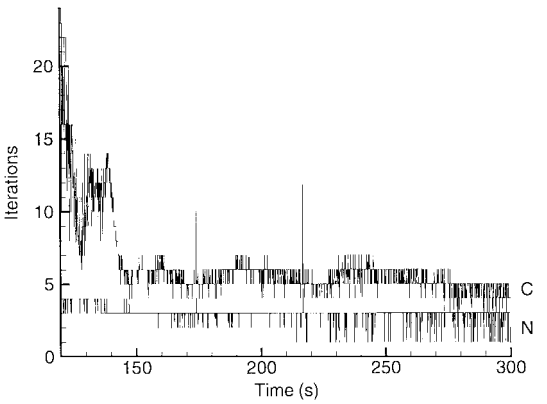

Fig. 15 Number of iterations required for convergence of the FADS algorithm using different pressure models.

error is not stated in Ref. 7.) The results from the wind-tunnel calibrated SEADS are, thus, of comparable accuracy to those of the CFD-calibrated HYFLEX FADS.

The final air data parameter to be investigated is the freestream static pressure P_∞. Figure 13 shows the FADS predictions of P_∞, along with a value based on the HYFLEX trajectory and meteorological data. The CFD–FADS estimate is observed to be poor, whereas the Newtonian–FADS estimate is much worse. After examination of Eq. (13) [or Eq. (11)], the cause of the bad P_∞ estimates becomes apparent. At hypersonic flight conditions, the P_∞ term is dwarfed by P_{gt}. Because of the disparity in relative magnitudes, it is very difficult to accurately resolve both quantities simultaneously. Small amounts of error or noise in the surface pressure measurements further compound the problem. Examples of this kind of error include the pneumatic lag in the tubing connecting pressure ports to sensors, pressure port angular misalignment resulting from the deformation of the nose cap at high temperature, and sensor error itself.

The error in predicting P_∞ consequently causes error in R [Eq. (14)]. Because R is used to determine many of the parameters in the CFD pressure correction model, the CFD–FADS prediction of other air data parameters (besides P_∞) might thus be expected to suffer. Contrarily, Figs. 8–12 show that the CFD–FADS results are quite good. Good results are still obtained because the core curve-fit coefficients in the CFD pressure model [c_k in Eq. (16)] are independent of R.

By using satellite positioning and meteorological data, it is possible to make a reasonably accurate estimate of P_∞. If these data are available onboard the vehicle, they can be used as a supplement to help improve the accuracy of the FADS air data estimates. To investigate this technique, the FADS algorithm was tested with P_∞ constrained to meteorological estimates. All of the results shown in Figs. 8–10 did not change appreciably. However, the Newtonian–FADS prediction of q_∞ did show significant improvement. By constraining P_∞, the quality of the pressure model fit becomes less important in determining the magnitude of P_{gt} and, consequently, q_∞.

The size of the pressure residuals [E_i^* in Eq. (2)] is a useful indicator of how well the pressure models fit the measured data. A residual of zero implies a perfect fit. Shown in Fig. 14 are the root mean square pressure residuals for the nine nose pressure sensors, expressed as a percentage of freestream dynamic pressure. For both pressure models, erratic results are observed early in the flight, where the air density is low, the vehicle has greatest speed, and high-temperature gas effects are strong. Thus, it may be concluded that the pressure measurements, the pressure models, or both lose accuracy at the more extreme flight conditions. Later in the flight, the CFD pressure model displays a residual consistently smaller than the modified Newtonian pressure model.

Algorithm Convergence and Stability

Figure 15 shows the number of iterations required for convergence of the air data inversion algorithm. All air data parameters from state estimate $j + 1$ must differ by less than 0.001% (or 1×10^{-4} deg) from estimate j before convergence is obtained [see Eq. (3)]. The Newtonian–FADS takes about three iterations to reach convergence, whereas the CFD–FADS requires at least an extra two iterations. To understand why, consider the first-order Taylor series expansion in Eq. (5). By using this expansion, we are assuming that the pressure model behaves linearly about a particular air data state. The CFD pressure model, being more complex (and farther from linear) than the modified Newtonian model, is adversely affected by the linearization to a greater extent. Thus, the absence of high-order terms in Eq. (5) means that the inversion algorithm requires extra iterations to achieve convergence when the CFD pressure model is used. The overall speed of the CFD–FADS running on a MIPS R10000 195-MHz processor was 370 Hz. The corresponding speed for the Newtonian–FADS algorithm was 1270 Hz. Both speeds are in excess of 50 Hz, which is the typical in-flight requirement for a hypersonic vehicle air data system.[2]

The singular values of the design matrix $\boldsymbol{A}$ provide a convenient way to check the stability of the air data solution technique. Singular values of zero indicate that column degeneracies exist in $\boldsymbol{A}$ and that there are linear combinations of air data parameters that are ill determined by Eq. (4). To obtain meaningful and stable solutions from the air data system algorithm, it is important that all singular values remain significantly larger than machine precision. The condition number of $\boldsymbol{A}$ is also a useful indicator of solution stability and is defined as the ratio of its largest and smallest singular values. A low condition number is desirable, and a condition number of infinity implies that the matrix is singular. Using the modified Newtonian pressure model, the worst (largest) design matrix condition number encountered was 1.24×10^5, whereas the worst (smallest) singular value was 0.49. For the CFD-calibrated pressure model, the worst condition number and singular value were 7.23×10^4 and 0.53, respectively. Thus, the CFD-calibrated pressure model poses a better-conditioned air data inversion problem. Additionally, the condition numbers and singular values of $\boldsymbol{A}$ lie well within machine precision for both pressure models.

In testing, the FADS algorithm proved to be robust and converged for all of the sets of pressure data for both pressure models. This is despite a number of data spikes being present in the input data. The effect of these input spikes on air data prediction is clearly seen in the displayed results. Previous investigators have encountered instability problems when the edge of the bow sonic zone nears or crosses pressure port locations.[4] For the HYFLEX flight, the sonic line crosses the outer transverse pressure ports (ps7 and ps9) at about 270 s after flight commencement. No perturbations in results or algorithm stability problems are observed at this time.

Conclusions

A technique for calibrating the HYFLEX vehicle FADS was described. The calibration involved using CFD simulation to provide the FADS algorithm with an accurate pressure model. No experimental or flight pressure data were used to augment the CFD pressure model. Using the pressure data recorded during the HYFLEX flight, we compared air data predictions from the calibrated FADS to those obtained from a FADS based on the modified Newtonian pressure model. The main findings were as follows:

1) The CFD-calibrated FADS predicted the vehicle angle of attack and angle of sideslip to approximately the accuracy required for control of a broad-envelope, hypersonic vehicle. Dynamic pressure was predicted to an accuracy better than or equal to that of the onboard IMU.

2) The modified Newtonian–FADS estimates of angle of attack and dynamic pressure did not meet the accuracy required for vehicle control. The modified Newtonian–FADS angle-of-sideslip estimates were close to those made by the CFD-calibrated FADS.

3) Both the uncalibrated and calibrated FADS gave poor estimates of the freestream static pressure.

4) The experimental calibration of air data system pressure models is not mandatory. Numerical results alone were sufficient to generate a good pressure model for the HYFLEX FADS in hypersonic flight.

5) The numerical calibration procedure produced results of accuracy comparable to that obtained by procedures that use wind-tunnel data, such as in the SEADS calibration.

6) The nonuniformity in radius of the HYFLEX nose made the CFD–FADS calibration more difficult. Also, the nonuniformity was the predominant cause of error in the angle-of-attack predictions made by the uncalibrated FADS. In the future, it would be beneficial to position all pressure ports on a symmetric region of the nose.

References

[1]Johnston, I. A., Tuttle, S. L., Jacobs, P. A., and Shimoda, T., "The Numerical and Experimental Simulation of Flow Around the HYFLEX Vehicle Forebody," *Proceedings of the 21st International Symposium on Shock Waves*, edited by A. Houwing, Vol. 1, Panther Publishing, Canberra, Australia, 1997, pp. 453–511.

[2]Benser, E. T., "Air Data Measurement for Hypersonic Vehicles," Society of Automotive Engineers TP Series, SAE Paper 912143, Sept. 1991.

[3]Whitmore, S. A., Moes, T. R., and Leondes, C. T., "Development of a Pneumatic High-Angle-of-Attack Flush Airdata Sensing (HI-FADS) System," *Integrated Technology Methods and Applications in Aerospace Systems Design*, edited by C. Leondes, Vol. 52, Control and Dynamic Systems—Advances in Theory and Applications, Academic, San Diego, CA, 1992, pp. 453–511.

[4]Whitmore, S. A., Davis, R. J., and Fife, J. M., "In-Flight Demonstration of a Real-Time Flush Airdata Sensing (RT-FADS) System," NASA TM-104314, Oct. 1995.

[5]Whitmore, S. A., and Moes, T. R., "Measurement Uncertainty and Feasibility Study of a Flush Airdata System for a Hypersonic Flight Experiment," NASA TM-4627, June 1994.

[6]Pruett, C., Wolf, H., Heck, M., and Siemers, P., "An Innovative Air Data System for the Space Shuttle Orbiter: Data Analysis Techniques," AIAA Paper 81-2455, Nov. 1981.

[7]Wolf, H., Henry, M. W., and Siemers, P. M., "Shuttle Entry Air Data System (SEADS): Optimization of Preflight Algorithms Based on Flight Results," AIAA Paper 88-2053, May 1988.

[8]Johnston, I. A., Tuttle, S. L., Jacobs, P. A., and Shimoda, T., "The Numerical and Experimental Simulation of Hypervelocity Flow Around the HYFLEX Vehicle Forebody," *Shock Waves* (to be published).

[9]Inouye, Y., Watanabe, S., Fujii, K., Ohtake, K., Takaki, R., Takizawa, M., Ito, T., Shirouzu, M., Kai, T., and Teraoka, K., "Quick Report of HYFLEX Onboard Measurements," 20th International Symposium on Space Technology and Science, Paper 96-d-09, Gifu, Japan, May 1996.

[10]Ishimoto, S., Takizawa, M., Suzuki, H., and Morito, T., "Flight Control Design of Hypersonic Flight Experiment (HYFLEX) Vehicle," 20th International Symposium on Space Technology and Science, Paper 96-f-07, Gifu, Japan, May 1996.

[11]Johnston, R. L., *Numerical Methods*, Wiley, New York, 1982, pp. 76–86.

[12]Johnston, I. A., and Jacobs, P. A., "SF2D: A Shock Fitting and Capturing Solver for Two Dimensional Compressible Flows," Dept. of Mechanical Engineering, TR 6/96, Univ. of Queensland, Brisbane, Australia, July 1996.

[13]Anderson, W., Thomas, J., and van Leer, B., "A Comparison of Finite Volume Flux Vector Splittings for the Euler Equations," AIAA Paper 85-0122, Jan. 1985.

[14]Wada, Y., and Liou, M.-S., "A Flux Splitting Scheme with High-Resolution and Robustness for Discontinuities," AIAA Paper 94-0083, Jan. 1994.

[15]Gupta, R. N., Yos, J. M., Thompson, R. A., and Lee, K.-P., "A Review of Reaction Rates and Thermodynamic and Transport Properties for an 11-Species Air Model for Chemical and Thermal Nonequilbrium Calculations to 30,000 K," NASA Ref. Pub. 1232, Aug. 1990.

[16]Hartung, L. C., and Throckmorton, D. A., "Computer Graphic Visualization of Orbiter Lower Surface Boundary-Layer Transition," *Journal of Spacecraft and Rockets*, Vol. 24, No. 2, 1987, pp. 109–114; also AIAA Paper 84-0228, Jan. 1984.

[17]Pap, R., Saeks, R., Lewis, C., Carlton, A., Kocher, M., and Kersting, T., "The LoFLYTE Program," AIAA Paper 98-1519, April 1998.

[18]NAL/NASDA HOPE Cooperative Research Team HYFLEX Subgroup, *Hypersonic Flight Experiment Handbook*, NN-95-3009, National Aerospace Lab. and National Space Development Agency, 1994 (in Japanese).

J. R. Maus
Associate Editor